

Structure of the Avian Mitochondrial Cytochrome bc_1 Complex

Edward A. Berry,¹ Li-Shar Huang,^{1,2} Zhaolei Zhang,^{1,3} and Sung-Hou Kim^{1,2,3}

Received May 12, 1999

There are now four structures of vertebrate mitochondrial bc_1 complexes available in the protein databases and structures from yeast and bacterial sources are expected soon. This review summarizes the new information with emphasis on the avian cytochrome bc_1 complex (PDB entries 1BCC and 3BCC). The Rieske iron-sulfur protein is mobile and this has been proposed to be important for catalysis. The binding sites for quinone have been located based on structures containing inhibitors and, in the case of the quinone reduction site Qi, the quinone itself.

KEY WORDS: Ubiquinol:cytochrome c oxidoreductase; membrane protein; electron transfer; structure determination.

INTRODUCTION

Structures determined by X-ray diffraction have now been deposited in the Protein Data Bank for the mitochondrial bc_1 complex from tetragonal crystals of the bovine enzyme (Xia *et al.*, 1997), orthorhombic crystal of the chicken enzyme (Zhang *et al.*, 1998), and two different hexagonal space groups of the bovine enzyme (Iwata *et al.*, 1998). While all three structures are of relatively low resolution (Table I), they tend to be strongest in different areas of the molecule, and combined we have a tremendous amount of new structural information about this respiratory chain complex to assimilate. This report outlines some of the new

information, with emphasis on the avian structure determined in the authors' laboratory.

SUMMARY OF THE STRUCTURE DETERMINATION

The cytochrome bc_1 complex was isolated from chicken heart mitochondria by extraction with dodecylmaltoside, ion-exchange chromatography on DEAE-Sepharose CL6B, and gel filtration on Sepharose CL6B. The final pooled fractions were concentrated by ultrafiltration through Amicon YM-100 membranes and crystallized with PEG as precipitant at slightly acidic pH and low ionic strength (~ 100 mM). The crystals were equilibrated with a glycerol-based cryoprotectant solution, containing, in some cases, heavy atom reagents, and flash-frozen in liquid nitrogen or ethane for X-ray diffraction data collection.

The diffraction data was phased by multiple isomorphous replacement, with the best phasing power from a trimethyl-lead derivative. The low-resolution MIR¹ phases were improved and extended by density modification including multicrystal and noncrystallographic symmetry averaging, using three other crystal forms, two from beef and one from rabbit. The chicken

¹ E. O. Lawrence Berkeley National Laboratory, University of California, Berkeley, California 94720.

² E. O. Lawrence Berkeley National Laboratory, Department of Chemistry, University of California, Berkeley, California 94720.

³ E. O. Lawrence Berkeley National Laboratory, Graduate Group of Physics, University of California, Berkeley, California 94720.

⁴ E. O. Lawrence Berkeley National Laboratory, Department of Chemistry, Graduate Group of Physics, University of California, Berkeley, California 94720.

⁵ Abbreviations used: MIR, multiple isomorphous replacement method; PDB, Protein Database; F_o , structure factor amplitude (observed); F_c , structure factor (calculated); I, diffraction reflection intensity; B factor, temperature factor.

Table I. Cytochrome *bc*₁ Complex Structures From Three Groups

Group	Texas/Oklahoma	Berkeley	Uppsala	
Reference	<i>Science</i> 287 , 60 (July 1997)	<i>Nature</i> 392 , 677 (April 1998)	<i>Science</i> 291 , 64 (July 1998)	
Protein source	Beef heart	Chicken heart	Beef heart	
PDB Entry	1QCR	1BCC	1BE3	1BGY
Space Group	<i>I</i> ₄ 22	<i>P</i> ₂ ₁ 2 ₁ 2 ₁	<i>P</i> ₆ ₅ 22	<i>P</i> ₆ ₅
Resolution	2.7	3.16	3.0	3.0
Number unique refl. used in refinement ^a	72196 (73.5%)	107167 (83.6%)	72948 (81.5%)	101111 (73.7%)
Effective Resolution ^b	3.0	3.35	3.22	3.32
R-free	0.37	0.31	0.32	0.36
Final released model contains:	C α for eleven chains, (Cyt. <i>c</i> ₁ only C-term) Fe ₂ S ₂ , 1 heme	Full model for nine chains Fe ₂ S ₂ , 3 hemes, 2 PL, 1 deterg, 1 quinone	Full Model for eleven chains Fe ₂ S ₂ , 3 hemes	

^a Reflections used in refinement included all reflections with $F > 2\sigma(F)$ for the Texas and Berkeley groups and all reflections with $F > 0$ for the Uppsala group.

^b "Effective resolution" is a resolution such that a complete data set with the same cell parameters and extending to that resolution would have the same number of reflections as the number of reflections in the data set (Stonehuerner *et al.*, 1985).

^c Temperature factors are not compared because in at least three of the structures the final model was refined against data in which the temperature factor had been modified.

crystals and the beef monoclinic crystals each have two-fold noncrystallographic symmetry, giving six independent maps of the complex for molecular averaging. A model was built into the improved maps and refined against several of the best datasets. Data and refinement statistics for some of the datasets on which this report is based are given in Tables II and III. The structure of the uninhibited chicken cytochrome *bc*₁ complex (deposited coordinates entry 1BCC) is shown in Fig. 1.

MOVEMENT OF RIESKE PROTEIN-ELECTRON TRANSFER BY DOMAIN MOVEMENT

During multicrystal averaging it became clear that the extrinsic domain of the Rieske protein occupied slightly different positions in the different crystals forms. The locations of heme and nonheme irons, determined from anomalous scattering or as the highest peaks in a conventional density map, showed that the iron-sulfur cluster was in a different position relative to the hemes in the different crystals (Fig. 2). When the chicken crystals were made from protein inhibited by stigmatellin, the location of the iron-sulfur cluster was markedly different, closer to cytochrome *b* and farther from cytochrome *c*₁ than in the native crystals. This position, however, turned out to be the same as that determined by the Deisenhofer group from native

beef *bc*₁ crystals of the tetragonal form developed by Yu and co-workers. This together with relatively poor order of the iron-sulfur protein in the latter crystals (Xia *et al.*, 1997) suggested that the cluster-containing extrinsic domain of the Rieske protein was mobile. This, in turn, provided a solution for the problem that in all crystal forms the iron-sulfur cluster was too far from either its electron donor or acceptor for electron transfer through this center to occur at a kinetically competent rate. It was concluded that mobility of the Rieske protein may be important for its catalytic activity and it was proposed (Zhang *et al.*, 1998; Kim *et al.*, 1998) that electron transfer from quinol at the Q_o site occurred with the Rieske protein in the position seen in the chicken crystals with stigmatellin or the native tetragonal beef crystals, while electron transfer to cytochrome *c*₁ occurred from the position seen in the beef *P*₆₅22 crystals. These two conformations are illustrated in Fig. 3. Biochemical indications that suggest movement of the Rieske extrinsic domain is required for catalytic activity have come from a spontaneous mutation whose effect can best be explained as blocking movement (Gießler A., di Rago, J.-P., Hagen, W., Link, Th. A., von Jagow, G., Slonimski, P. P., and Brandt, U., personal communication.) and from site-directed mutations designed to block movement in order to test the hypothesis (Tian *et al.*, 1998, 1999).

What drives the movement of the Rieske protein? It is not yet clear whether the movement of the Rieske protein is coupled to other events in the catalytic cycle,

Table II. Datasets Used in Avian *bc*₁ Complex Structure Determination

Dataset Name ^a	Cell parameters			Resolution, redundancy, completeness, precision					Temperature factor ^b				
	A	b	c	<i>d</i> _{min}	Measurements	Unique reflections (completeness)	R-sym ^c (<i>I</i> > -3σ)	In shell 3.5–3.6 Å ^a	Completeness (<i>F</i> > σ _F)	Overall	B11	B22	B33
1BCC	169.582	182.521	240.577	3.16	556,456	123,869 (0.916)	0.102	9.6	0.99	25.9	83.5	17.3	17.5
3BCC	173.178	179.727	238.220	3.20	394,429	111,849 (0.910)	0.243	2.9	0.93	33.0	57.9	29.3	25.1
STG	173.464	182.448	241.328	3.00	306,685	117,928 (0.771)	0.131	4.0	0.76	20.4	35.9	14.4	20.0
MYX	173.177	181.217	240.003	3.40	365,806	90,815 (0.871)	0.228	3.3	0.89	22.2	59.0	13.4	14.4
MOS	171.838	181.925	240.412	3.59	159,573	70,736 (0.741)	0.203	—	0.00	29.7	59.0	31.2	22.3

^a The data set 1BCC is from a crystal with no inhibitors and 3BCC is from one with antimycin and stigmatellin. STG, ANT, MYX, and MOS are from crystals with stigmatellin (SIG), antimycin (AMY), myxothiazol (MYX), and MOA-stilbene (MOS) respectively. The asterisk on 1BCC and 3BCC indicates the initial refinement of these data sets used for the coordinates submitted in Spring 1998 and released July 1998.

^b The isotropic overall B factor was estimated by scaling each dataset against structure factors calculated from the model of the native *bc*₁ complex (1BCC) in which all atomic B factors were set to 20. The relative B factor obtained was added to 20 to give the B factor for the crystal. Anisotropic temperature factors B11, B22, and B33 were determined by scaling the raw data set against *F*_{calc} as described above, but using anisotropic scaling. Atomic B factors in the coordinates were obtained by refining against the original *F*_{obs}, which had not been subjected to any adjustment of the B factor, such as “sharpening” or scaling in which B factor as well as scale is modified. This is not true of the refinements 1BCC* and 3BCC*, which are on arbitrary B factor scales.

^c In calculating R-sym, reflections with negative measured intensity were not rejected unless the absolute value was greater than 3σ. Therefore, the R-sym value is very high in the highest-resolution shells where the intensity of most reflections is below the noise level and should not be compared with R-sym values calculated after excluding weak rejections. The French and Wilson method (Ludwig *et al.*, 1983) as implemented in the CCP4 program truncate, was used to estimate maximum likelihood values of *F* and σ_F from all reflections, including those with negative intensity. Only reflections with *F* > 2σ_F were used in refinement.

^d Average *F*/σ_F and completeness were calculated in a narrow shell around 3.5 Å (shell slightly different for each data set). *F* was calculated from *I* by the truncate method (see Materials and Methods). Completeness was calculated excluding those reflections for which *F* < σ_F.

Table III. Structure Refinement Statistics for Crystal Datasets

Dataset name ^a	Data refinement											
	<i>D</i> _{min} (refine)	Reflections used (<i>F</i> ₀ > 2σ <i>F</i> ₀)	<i>D</i> _{min} ^b (effective)	No. atoms in model	Data ^c parameters	R-free value	Coordinate error ^c	⟨ <i>B</i> _{atomic} ⟩ _{cyt.b}	Q _i site occupant	⟨ <i>B</i> _{atomic} ⟩ _{Q_i} occupant	Q _o site occupant	⟨ <i>B</i> _{atomic} ⟩ _{Q_o} occupant
1BCC*	3.16	107167	3.35	31444	1.70 (0.85)	0.310	0.56	65.6	U10	81	—	—
1BCC	3.16	121980	3.21	31444	1.94 (0.97)	0.322	0.69	48.7	U10	71	—	—
3BCC*	3.5	71026	3.85	31530	1.13 (0.56)	0.321	0.56	46.	AMY	37	STG	37.
3BCC	3.2	104521	3.38	31530	1.66 (0.83)	0.323	0.91	46.7	AMY	37	STG	28.
STG	3.0	115822	3.30	31514	1.84 (0.92)	0.297	0.61	44.4	U10	62	STG	28.
MYX	3.40	88208	3.60	31510	1.40 (0.70)	0.315	0.73	30.8	U10	64	MYX	15.
MOS	3.59	68462	3.92	31488	1.09 (0.54)	0.321	0.71	39.65	U10	75	MOS	18.

^a See Table II footnote a.

^b “Effective resolution” is a resolution such that a complete dataset with the same cell parameters and extending to the resolution that would have the same number of reflections as the number of reflections in the dataset in question greater than two times the sigma level (Stonehauer *et al.*, 1985)

^c The data to parameters ratio is calculated as the ratio of reflections to 4 times the number of atoms in a monomer or (dimer). The factor of four is because *x*, *y*, and *z* coordinates and B factor are refined for each atom. Because we used noncrystallographic constraints to link atoms in different monomers, the number of atoms in a monomer is more appropriate.

^d Coordinate error is the ESD from cross-validated SigmaA treatment over the same resolution range and using the same bulk solvent correction as used in refinement.

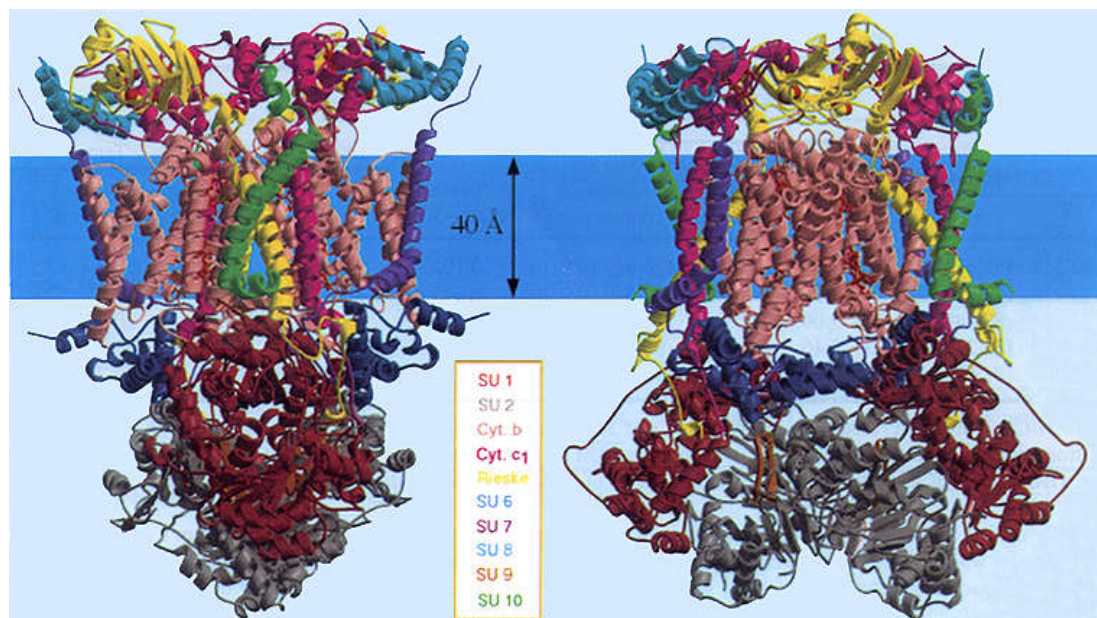


Fig. 1. The structure of avian cytochrome bc_1 complex. An overall view of the ten-subunit complex from two orientations. The dimer two-fold axis is vertical in the plane of the page. The shaded band represents the approximate location of the membrane hydrophobic phase, with the mitochondrial matrix below and intermembrane space above. Ten subunits are shown. Subunit 11, if it exists in the chicken complex, is not present in the crystals and not consistently present in the preparation of the enzyme. This figure was made from PDB entry 1BCC, first revision after release.

such as oxidation and reduction of certain redox centers, or results from simple diffusion of the extrinsic domain between different binding sites, limited by its connection to the transmembrane helix. Movement in response to other events in the cycle would fit well with the previous hypothesis of a “catalytic switch” mechanism for gating electrons from the Q_o site onto either the Rieske cluster or cytochrome b to ensure the bifurcated reaction at center Q_o (Brandt and von Jagow, 1991; Brandt *et al.*, 1991). Furthermore earlier proposals of conformational changes related to the occupant at the Q_i site or the redox state of cytochrome b (Rieske *et al.*, 1967) suggested a general mechanism for the switching. However the flexible “neck” connecting the extrinsic domain of Rieske to its transmembrane helix would not seem to provide a vehicle for transmission of a conformational change and there is no direct evidence for a conformational change related to the redox state of cytochrome b or the occupant of the Q_i site. Additional information about the effect of inhibitors on the mobility, discussed elsewhere in this volume, was provided by the Deisenhofer group (Kim *et al.*, 1998).

We have looked for the proposed conformational change induced by antimycin at the Q_i site (Rieske *et al.*, 1967). We compared the structures of cytochrome

b from four crystals: the uninhibited structure 1BCC, the antimycin 1 stigmatellin structure 3BCC, the stigmatellin-inhibited structure 2BCC, and a third undeposited structure with antimycin only. Making the four possible pairwise comparisons gives the effect of antimycin in the presence or absence of stigmatellin and the effect of stigmatellin in the presence or absence of antimycin. The comparison was carried out by superimposing the C- α atoms of the different structures. Initially all residues were used. Then, when it was clear where the conformational changes occurred, these residues were omitted in superimposing. With the structures thus superimposed the distance between corresponding C- α atoms in two structures was measured and plotted versus residue number (Fig. 4). Stigmatellin in the presence (green trace) or absence (blue) of antimycin induced significant correlated changes of up to 2.3 Å. These involve mainly the α -cd1 and α -cd2 helices and the α E- α F linker and can be seen in the superimposed electron density of crystals 1bcc and 3bcc in Fig. 5. These changes are probably due to (1) these structures being pressed by the Rieske protein in its cytochrome b position and to (2) opening of the Q_o pocket in order to accommodate stigmatellin. It remains possible, however, that these conformational changes are the result of a catalytic switch and that

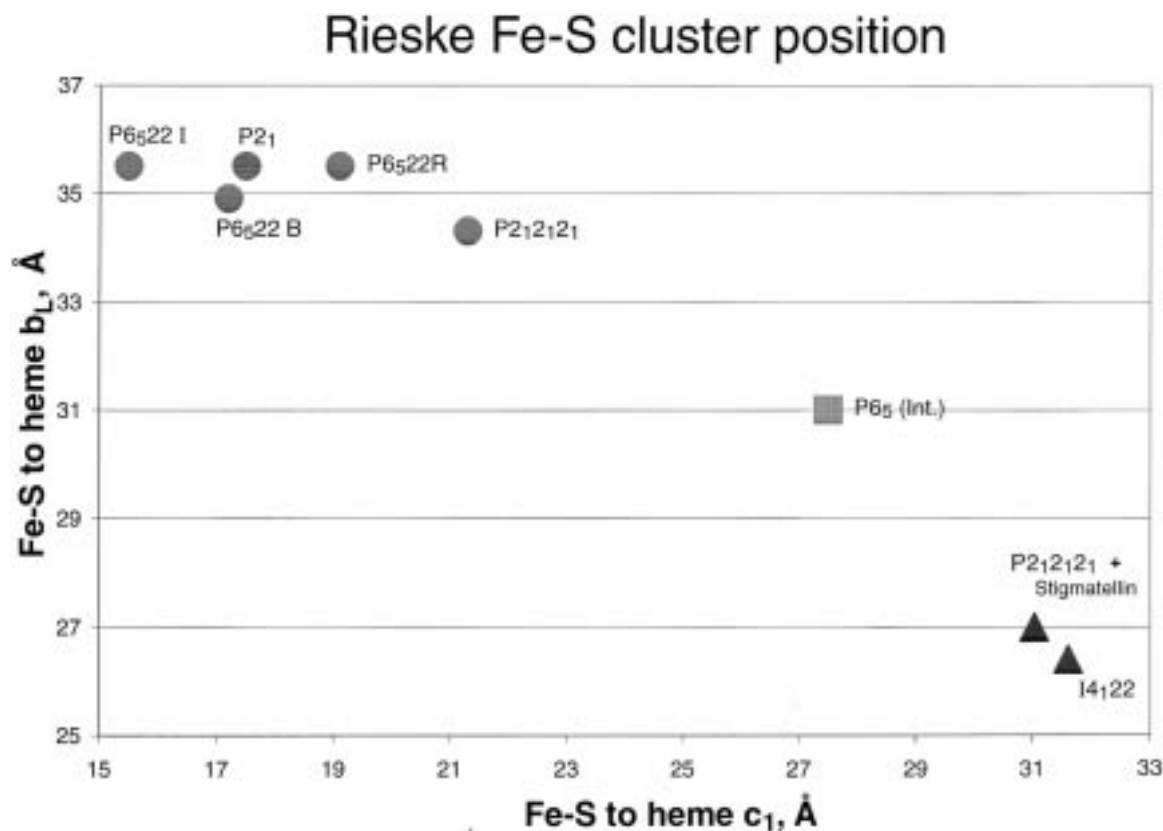


Fig. 2. Different positions of the Rieske iron–sulfur cluster relative to heme irons. Iron–iron distances are taken from references Xia *et al.* (1997), Zhang *et al.* (1998), and Iwata *et al.* (1998). The distance between the Rieske cluster and the low potential heme of cytochrome b is plotted on the vertical axis and that to the heme of cytochrome c_1 on the horizontal axis. *Triangles* represent positions approximating the cytochrome b position, *solid circles* approximate the cytochrome c_1 position, and the *squares* represents the intermediate position found in one monomer of the $P6_5$ crystal. The data labels identify the following structures: $I4_122$, entry 1QCR [bovine tetragonal (Xia *et al.*, 1997)]; chicken + stigmatellin, entry 3BCC; $P6_5$, entry 1BGY, chain E (Iwata *et al.*, 1998); $P2_12_12_1$, entry 1BCC (chicken); $P6_522R$, rabbit hexagonal (Zhang *et al.*, 1998); $P2_1$ beef monoclinic (Zhang *et al.*, 1998); $P6_522B$, bovine hexagonal (Zhang *et al.*, 1998); $P6_522I$, entry 1BE3 [flash-frozen, dehydrated beef hexagonal (Iwata *et al.*, 1998)].

they, in turn, destabilize binding of the Rieske protein in the cytochrome b position.

Antimycin in the presence of stigmatellin (red) induced no changes greater than 0.5 Å, which is below the rms coordinate error expected from cross-validated sigma-A treatment. Antimycin versus native (purple) shows larger changes of up to 1 Å, but they do not correlate with the changes induced by antimycin in the presence of stigmatellin and are probably due to the less well-determined refinement against the weak antimycin dataset. We conclude that antimycin induces no significant conformational change within the accuracy of these structures.

A noncrystallographic technique for evaluating the orientation of the Rieske protein has been found in the direction dependence of the epr signal from the Rieske Fe–S cluster (Brugna *et al.*, 1998) in oriented

layers. From the X-ray structures, the Fe_1 – Fe_2 vector is roughly parallel to (8–11° from) the dimer twofold axis (and the perpendicular to the membrane) in the cytochrome b position, but it is about 70° from the twofold axis in the cytochrome c_1 position. While this technique would seem applicable only to the reduced, paramagnetic state of the Rieske cluster, it can be used to determine the position of the oxidized protein as well by using gamma irradiation to reduce the cluster after it has been frozen into its oxidized position by dehydration and low temperature. This work suggests that the redox state of the Rieske cluster affects its position (Brugna *et al.*, 1998).

Single-crystal epr experiments would seem an even better technique, but are complicated by the crystallographic symmetry in nontrigonal space groups. In the orthorhombic chicken crystals with stigmatellin

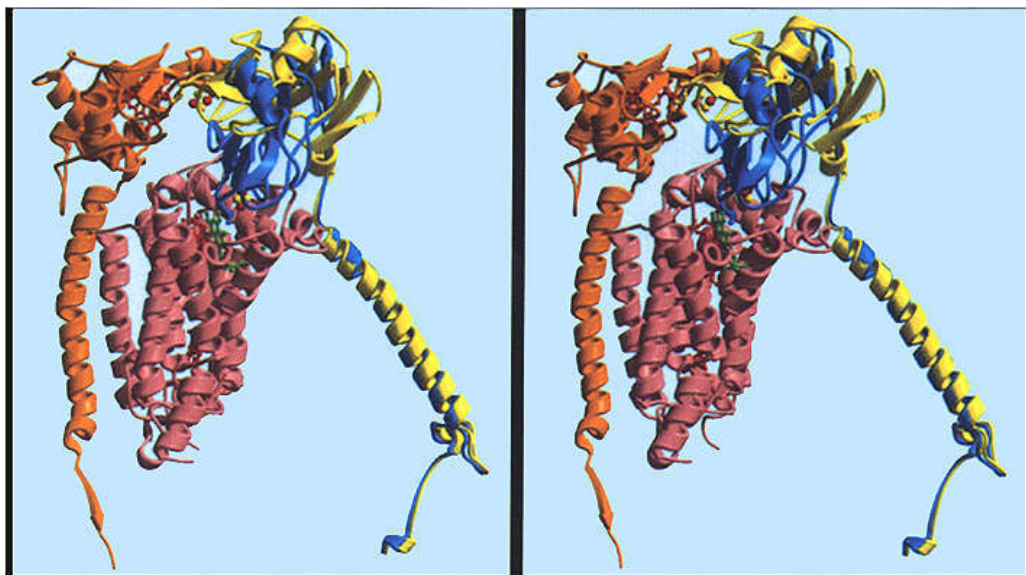


Fig. 3. Two conformations of the Rieske iron–sulfur protein (stereo pair). Cytochrome *b* (salmon) and the Rieske protein in the cytochrome *b* position (blue) are from PDB entry 3BCC. Cytochrome *c*₁ (orange) and the Rieske protein in cytochrome *c*₁ position (yellow) are from our unsubmitted beef *P*₆₅₂₂ structure (2). Stigmatellin (green) marks the position of the Q_o site and the hemes of cytochrome *b* and cytochrome *c*₁ are red. The iron–sulfur cluster in each position is shown as large red and yellow balls and H161 is solid blue (*b* position) or yellow (*c*₁ position).

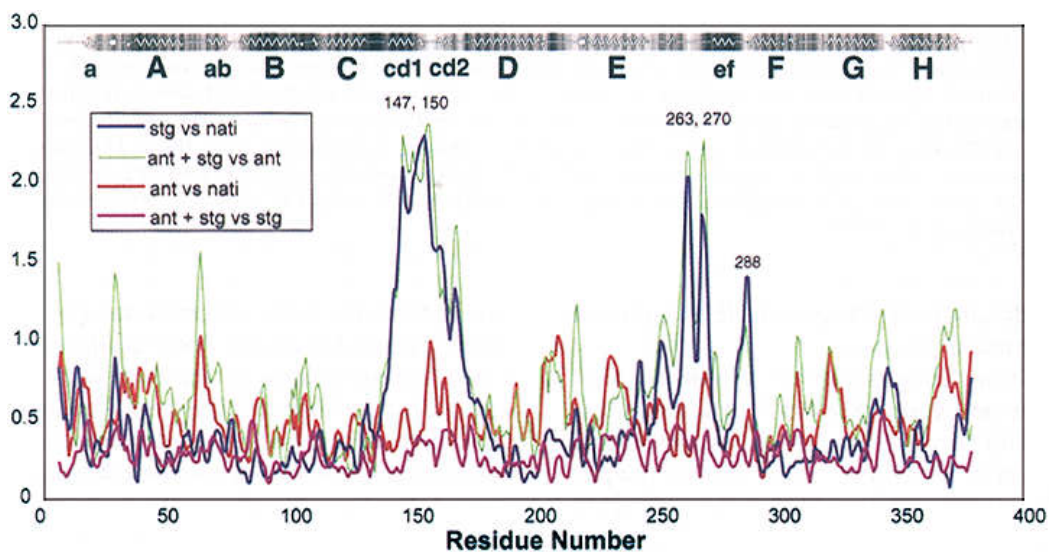


Fig. 4. Cytochrome *b* backbone movements induced by inhibitor binding. The structures of entry 1BCC (nati), 3BCC (stg 1 ant), and two unsubmitted datasets containing only stigmatellin (stg) or antimycin (ant) were superimposed so as to minimize the rms deviation of C- α atoms of residues 32–129, 180–248, and 294–380. Then the four pairwise comparisons indicated were made by subtracting the coordinates of corresponding C- α atoms in the superimposed structures. To reduce noise and emphasize changes involving more than a single residue, the resulting values were averaged in a window of three residues. The resulting value is plotted vs. residue number to indicate where the changes occur. A cartoon representing the secondary structure and surface exposure (prepared by the program Procheck) is aligned above.

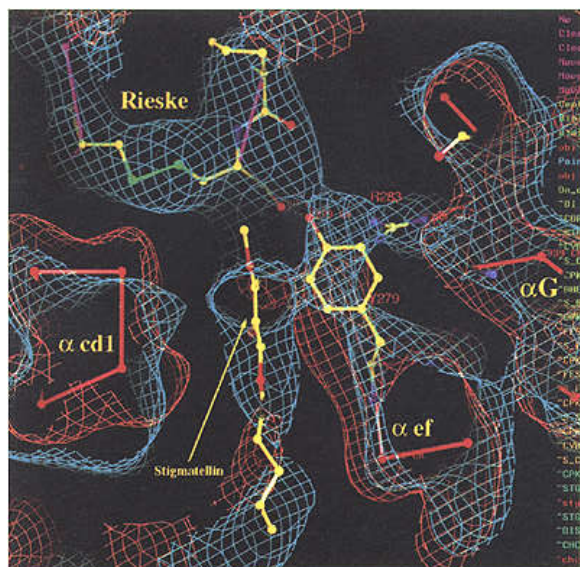


Fig. 5. Movements in the surface helices of cytochrome b in the presence of stigmatellin. The brown net is the electron density calculated from a native crystal (no inhibitors) and the red model is the backbone of cytochrome b built into this density. The blue net is density from a crystal containing stigmatellin. The purple backbone and connected side chains are the Rieske protein located in this density; the other ball-and-stick models depict stigmatellin and parts of cytochrome b . Both electron density maps are made using experimental phases after improvement by density modification and are contoured at 1 σ . The models are unrefined and intended only to identify features of the density. It can be seen that the $cd1$ helix moves down, perhaps pushed by the Rieske protein in docking and the ef helix and residue Y279 move to the right, perhaps as expansion of the Q_o site to accommodate stigmatellin. Rieske H161, which H bonds stigmatellin, is deep in the picture; the electron density can be seen dimmed by the depth cueing. The descending arm of the ef linker with P271 and E272 is not seen because it is in front of the slab of space used for the picture. Artifacts due to differences in cell parameters and different positioning of the protein in the two cells was avoided by transforming the models and skewing the maps to a reference cell in such a way as to optimally superimpose the rest of the protein.

(cytochrome b position), the dimer twofold is 118 from the crystallographic b axis, which puts the two Rieske Fe_1 – Fe_2 vectors 10 and 278 from the b axis and nearly perpendicular to the c axis. All symmetry-related dimers are rotated by 180° about one of the principle axes, which keeps the Fe – Fe vector nearly parallel to b and perpendicular to the c axis. A very clean angle-dependent w -band epr signal is observed (M. van Gastel and S. deVries 1997, unpublished). On the other hand, the uninhibited chicken crystals with the Rieske protein nearly in the cytochrome c_1 position have the Fe – Fe vectors at 171 and 228 from the crystallographic a axis, i.e., again along a principle axis, but this time

in opposite directions, but no clear angle-dependent signal was observed in preliminary experiments.

To explain the positions of the Rieske protein in the different crystals and epr experiments, assuming random diffusion between binding sites of different affinity, we would suggest the following. The strongest binding site is on cytochrome c_1 if the Q_o pocket is unoccupied, as in the native chicken crystals (Zhang *et al.*, 1998). The presence of quinone or stigmatellin at the Q_o site makes the cytochrome b position stronger, presumably because of a hydrogen bond from the Q_o site occupant to the Rieske H161 cluster ligand. This accounts for the cytochrome b position observed in the chicken crystals with stigmatellin (3BCC) and for partial occupancy of this position in the uninhibited tetragonal beef crystals (Xia *et al.*, 1997), which we must assume have the Q_o site partially occupied with quinone. Perhaps only the reduced Rieske binds tightly to the quinone-occupied Q_o site, which would account for the redox dependence of the epr signal direction in oriented membranes (Brugna *et al.*, 1998). Methoxyacrylate inhibitors of the Q_o site, such as myxothiazol and MOA-stilbene displace any endogenous ubiquinone and do not themselves bind to the Rieske protein, and so favor the cytochrome c_1 or the “free” position.

QUINONE-BINDING SITES

The structure and binding mode of the ubiquinone-binding sites is key to understanding the mechanism of the enzyme. Unfortunately, to date the cytochrome bc_1 preparations that give good crystals tend to be rather depleted in ubiquinone. In the chicken crystals, there is partial occupancy of the Q_i site. The deposited coordinates 1BCC have occupancy 0.79 for this quinone, but this is probably an overestimate. The actual occupancy is difficult to determine because of strong correlation between occupancy and temperature factor in refinement at low resolution. An indication of the position of ubiquinone at the Q_i site was also obtained from the tetragonal beef crystals (Xia *et al.*, 1997; Kim *et al.*, 1998) based on negative difference density between a crystal with antimycin and one without and the assumption that the density decrease is due to displacement of the quinone by antimycin. All three groups have good density for antimycin bound at the Q_i site. This is not surprising because the very high affinity for antimycin allows full occupancy and presumably improves the order. Coordinates for the chicken enzyme with antimycin bound are available

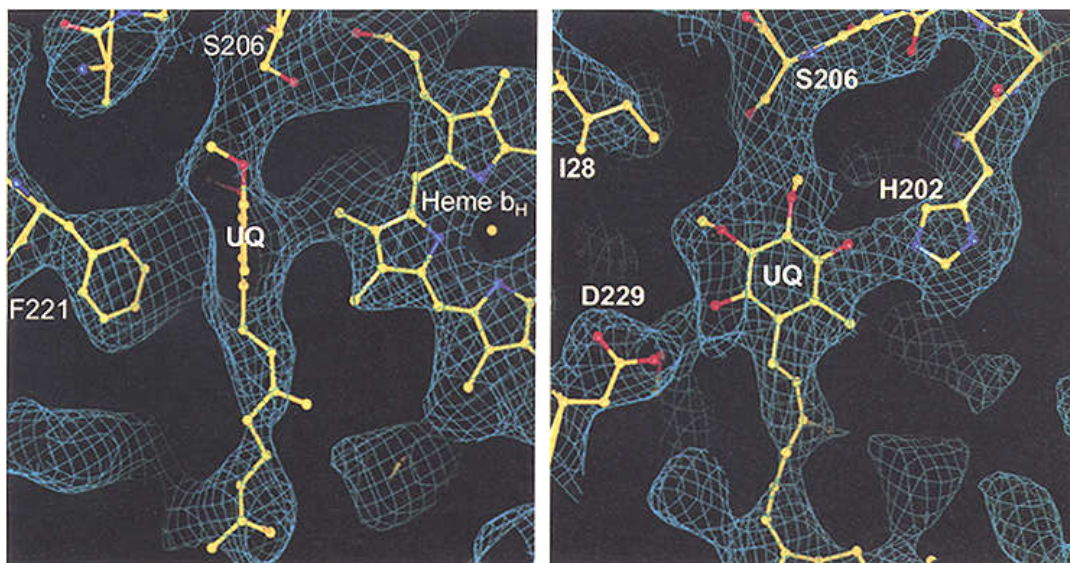


Fig. 6. Electron density at the Q_1 site in native chicken crystals. The refined model of the complex, superimposed on a $2F_o - F_c$ map, where F_o and F_c are calculated from the refined model with ubiquinone omitted to avoid phase bias, contoured at 1.1 σ . The superimposed model is the refined structure of the complex, including ubiquinone with its headgroup in the center of the figure. Panels A and B show two different views related by approximately 90° rotation about a vertical axis.

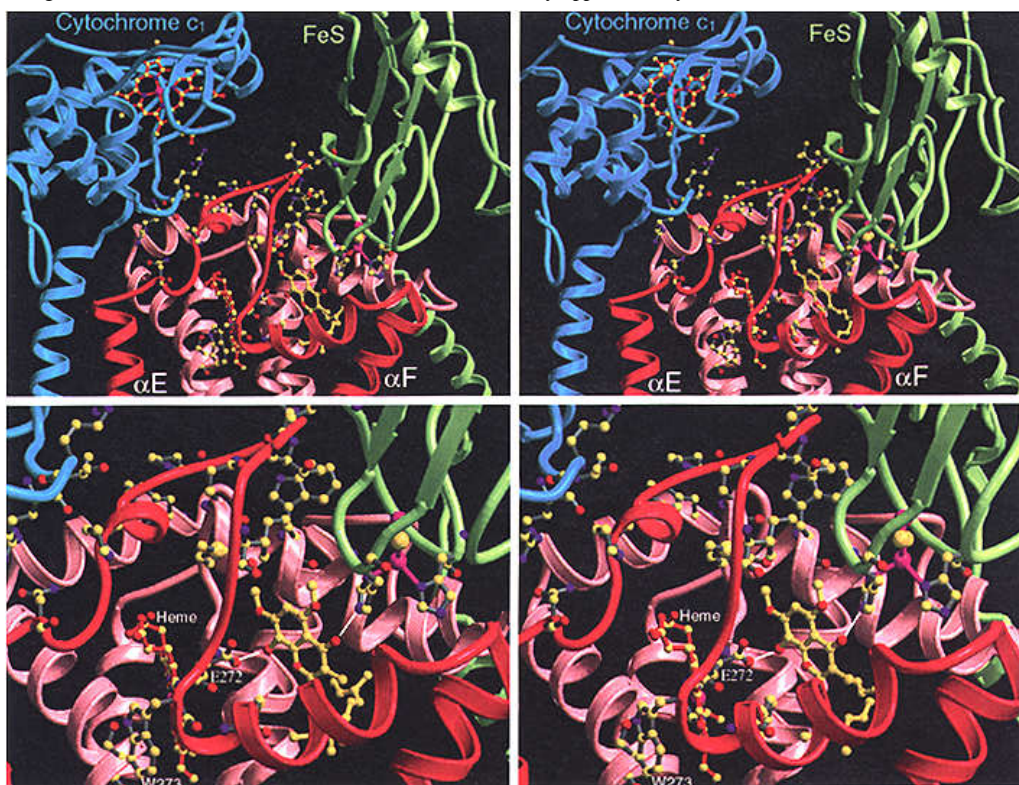


Fig. 7. Stereo view of the Q_0 site and the ef linker peptide. (Above), the view is zoomed out to show the region in the context of cytochrome *b* (pink and red), cytochrome *c*₁ (blue), and the Rieske protein (green). (Below), the view is zoomed in to make details visible. The transmembrane helices E and F of cytochrome *b*, as well as the connecting ef linker (residues 246–288) are red, while the rest of cytochrome *b* is pink. The binding position of Q_0 site inhibitors is shown by the yellow and red model of stigmatellin behind and to the right of the descending arm of the ef linker. Behind this inhibitor, the cd1 and C helices come together at an acute angle. Purple spheres are the iron atoms in the low-potential cytochrome *b* heme and in the Rieske iron–sulfur cluster. Some residues discussed in the text are labeled.

in entry 3BBC. No density has been reported for quinone at the Q_o site, therefore, we can only speculate on the binding of this substrate from the binding of inhibitors believed to bind as quinone analogs at the same site, such as stigmatellin for which coordinates are available in entry 3BCC.

Figure 6 shows our model and the supporting electron density for quinone at the Q_i site. Quinone binds between the heme and residues F221, H202, D229, S36, and S206, with the isoprenoid tail extending into the bulk lipid through a gap between L19 and M43. The strongest density connection to the protein is to H202. Specific hydrogen-bond interactions are a little uncertain at this resolution, but the density is consistent with the model of entry 1BCC, in which quinone hydrogen bonds with H202 and D229 by its carbonyl oxygens and with S206 by a methoxy oxygen. H202 was previously proposed to be a quinone ligand based on results of mutagenesis on the stability of the semiquinone at the Q_i site (Gray *et al.*, 1994). H202 and D229 are conserved throughout vertebrate, fungal, plant, and bacterial *bc*₁ complexes. F221, S206, and S36 are not well conserved. Antimycin binds with its aromatic salicylate ring in the same pocket but closer to D229 and farther from H202, forming no H bond with H202.

Q_o site inhibitors bind in a pocket between two elbows of protein, one formed by the transmembrane helix C with the cd1 surface helix and the other by the descending arm of the α E- α F linker (the conserved -PEWY- sequence) with the ef surface helix (Fig. 7). Stigmatellin binds at the Q_o site in van der Waals contact with the protein backbone around P271 and E272. There is a strong hydrogen bond to H161, a cluster ligand of the Rieske protein, which is in the proximal or cytochrome *b* position in the presence of this inhibitor. There is probably a hydrogen bond from the OH group on the other side of the ring to the side chain of E272. We can speculate that these two residues are the ligands for the hydroxyl oxygens of ubiquinol and that after oxidation of the quinol the protons are carried away by the Rieske protein and by E272, which in another conformation (in the absence of stigmatellin, PDB entry 1BCC) reaches into the hydrophilic region around the heme propionates which presumably equilibrates with the intermembrane aqueous phase. The distance from the carbonyl oxygen on the first ring of stigmatellin (O12 in structure 3BCC) to the methyl carbon of pyrrole ring A of the low potential heme is 10.1 Å.

Another class of Q_o-site inhibitors, the MOA (methoxyacrylate) inhibitors, binds somewhat differently. The methoxyacrylate group is closer to heme *b*_L (5.1 Å) and farther from Rieske binding site than is the ring of stigmatellin. The carbonyl end of the pharmacophore may hydrogen bond with the backbone N of E272 and/or with the phenolic OH of Y274. The other end of the pharmacophore may hydrogen bond with backbone atoms of G143 and A144 in helix C.

ARCHITECTURE OF THE α E- α F LINKER OF CYTOCHROME *b*: STAGING AREA FOR RIESKE AND CYTOCHROME *c*₁

Transmembrane helices E and F are on opposite sides of the *bc*₁ monomer. The polypeptide connecting them, depicted in Fig. 7, is interesting in a number of ways. It includes the residues of cytochrome *b* that are farthest from the membrane on the external (P) side and serves as part of the binding site for cytochrome *c*₁, for the Rieske Fe-S protein in both the cytochrome *b* and cytochrome *c*₁ positions, and for quinone analog inhibitors (and by inference for ubiquinone) at the Q_o site. It holds the Rieske protein and cytochrome *c*₁ together in the right orientation and distance for electron transfer, as well as stabilizing Rieske bound to the Q_o site. It may serve as a "guide" along which the Rieske slides in going between its two binding sites.

From residue 246 at the end of transmembrane helix E to residue 273 at the beginning of helix ef, the linker consists mainly of extended peptide with no secondary structure except one turn of 3-10 helix involving residues 254-257. Despite this, it is relatively well-ordered, with temperature factors only slightly higher than in the transmembrane helices.

At the end of helix E of cytochrome *b*, the side chain of residue F246 inserts between the N-terminal anchor loop and the C-terminal transmembrane helix of cytochrome *c*₁ (contacting residues P17 and G205). The polypeptide then turns upward out of the membrane and makes a single turn of 3₁₀-helix (residues 254-257), which is sandwiched between the N-terminal end of cytochrome *b* helix cd1 and residues 118 and 119 of cytochrome *c*₁. The ring of P259 makes hydrophobic contact with the aromatic ring of F64 in the ab helix. Thus, this part of the ef linker is supported by surface helices cd1 and ab, and, in turn, supports cytochrome *c*₁. It then continues up and over to the highest point from the membrane, residue 263-264. This section is supported mainly by H bonds from the

ring N of W142 and the side chain of Q138 (both these residues are completely conserved through bc_1 and b6f complexes) to the carbonyl oxygens of residues 264 and 261. Then it descends nearly perpendicular to the membrane to an elbow with the beginning of the ef helix, about 15 Å below the probable surface of the hydrophobic phase of the membrane. The angle of the elbow occurs at residue W273 of the highly conserved -PEWY- sequence, and a hydrogen bond connects the ring nitrogen of this residue to the side chain O γ of S89 in the middle of helix B. Both W273 and S89 are completely conserved, perhaps because this interaction is vital for positioning the elbow and the PEWY sequence, which forms part of the Q $_o$ quinone binding site. After the elbow, helix ef climbs at about 30° angle to the membrane and makes an elbow with transmembrane helix F at P286. This elbow is relatively disordered, with main-chain temperature factors greater by 35–40 Å² than in the buried elbow around W273.

CYTOCHROME c_1 : A CLASS I CYTOCHROME WITH SIMILARITIES TO CYTOCHROME c AND c_2 OR c_8

Although there is little sequence homology between mitochondrial or bacterial cytochrome c_1 and other cytochromes of Ambler's class I, the three-dimensional (3-D) structure is quite similar. This allows a structure-based sequence alignment and detailed comparison with other members of the class. The three alpha helices conserved in all class I cytochromes are present. The interconnecting protein segments are quite different.

Cytochrome c_1 was discovered in 1940 by Yakushiji and Okunuki (1940) and independently by Keilin and Hartree (1940) (as cytochrome e). It was present at 3.4 $\mu\text{mol/g}$ protein in Complex III isolated by Rieske *et al.* (1964). It was isolated in a subcomplex with subunit 8 by Yu *et al.* (1972). A preparation reportedly giving a single band was described by Konig *et al.* (1980). From this procedure, Kim and King (1981; 1987) developed improved preparations of 1- and 2-subunit cytochrome c_1 . Subunit 8 (the hinge protein for interaction of cytochrome c_1 and cytochrome c) was shown to be required for high-affinity binding of cytochrome c (Kim and King, 1981, 1983). Cytochrome c_1 was the second mitochondrial protein (after cytochrome c) to be sequenced (Wakabayashi *et al.*, 1980). The bovine cytochrome consists of 241 resi-

dues, with a hydrophobic section near the C-terminus (residues 204–222).

Wakabayashi *et al.* (1980) compared the sequence to that of cytochrome c and found two short stretches with significant similarity and, based on these, predicted the heme-binding residues. The N-terminal "fingerprint" CXXCH and preceding helix $\alpha 1$ region were correctly aligned, but the similarity around the proposed methionine heme ligand was coincidental (in fact, later sequences showed that methionine not to be conserved). There is really no significant sequence identity outside of the fingerprint and preceding region, although the similar N-terminal heme binding and spectral characteristics suggested homology. Often related proteins that have diverged to the point where little sequence identity remain still have very similar folding pattern, so the availability of X-ray structures for cytochrome c_1 was expected to clarify the relationship between cytochromes c_1 and c .

The bovine bc_1 structure from tetragonal crystals (Xia *et al.*, 1997; Kim *et al.*, 1998) is deficient in the intermembrane domains (subunit 8 and the extrinsic domains of the Rieske protein and cytochrome c_1 because of disorder in the crystals. These domains were better ordered in the orthorhombic crystals from chicken (Zhang *et al.*, 1998) and the hexagonal beef crystals (Iwata *et al.*, 1998). As expected, based on the high α -helix content predicted by CD spectroscopy, there was little similarity with cytochrome f , its functional analog in the b6f complex, however, there was sufficient similarity to cytochrome c and other class I cytochromes to make cytochrome c_1 a member of that class (Zhang *et al.*, 1998).

Figure 8 compares the structure of cytochrome c_1 and mitochondrial cytochrome c , the prototype of Ambler's class I cytochromes. The three helices labeled $\alpha 1$, $\alpha 3$, and $\alpha 5$ in the figure are present, in the same orientation to each other and to the heme, in all class I cytochromes and in cytochrome c_1 . Figure 9 gives another view of cytochrome c_1 and the hinge protein and compares the structures from the Berkeley and Uppsala groups.

The residues in these helices and the heme-binding regions can be used to superimpose cytochrome c_1 and other class I cytochromes. Once the superposition is established, a structure-based sequence alignment can be made by aligning those stretches that superimpose closely so that the aligned residues are the closest in space in the superposition. The results of two such alignments are shown in Fig. 10. Here the sequence of vertebrate cytochrome c_1 is aligned with

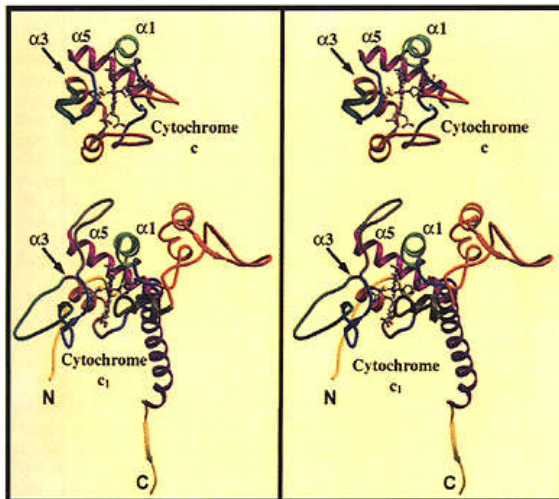


Fig. 8. Comparison of the structures of cytochrome c_1 and cytochrome c (stereo pair). (Above), ribbon diagram of mitochondrial cytochrome c in a standard orientation with the open C corner of the heme facing the viewer and the heme propionates directed downward. (Below), cytochrome c_1 rotated to put the common features between the two cytochromes in the same orientation. Corresponding segments of each cytochrome are drawn with the same color. Helices labeled $\alpha 1$, $\alpha 3$, and $\alpha 5$ correspond to similarly labeled helices in cytochrome c . The N- and C-termini are labeled in cytochrome c_1 .

mitochondrial cytochrome c from beef (above) and with bacterial cytochrome c_2 from *Rhodobacter capsulatus* (below). The aligned residues superimpose to within 1.0 Å in five regions of the sequence: the three helices mentioned above, residues around the two axial ligands, and the conserved -PNL- sequence starting at residue 30 in cytochrome c (PDL in cytochrome c_1).

Figure 11 combines structure-based alignments of vertebrate cytochrome c_1 and other class I cytochromes for which the structure is available with conventional alignments of other bacterial and fungal cytochromes c_1 . This shows conserved features of all class I cytochromes as well as suggesting the structural basis for the sequence differences between divergent cytochromes c_1 for which the structure is not yet available.

Only the helix $\alpha 1$ and the fingerprint region of cytochrome c_1 had sufficient sequence identity for correct alignment with cytochrome c , based on sequence alone. Highly conserved residues include (cytochrome c numbering) G6 at the contact point between helix $\alpha 1$ and helix $\alpha 5$, F/Y10, which is involved in interaction with Y/F97 in helix 5, and the fingerprint heme-binding residues CXXCH at 14–18. This latter feature is also conserved in nonclass I c -type cytochromes, however, in some protists, including euglenoids and trypanosomes, the first C is replaced by F and heme is bound by a single thioether linkage in both cytochromes c and c_1 (Mukai *et al.*, 1989).

Cytochromes c and c_2 and some other class I cytochromes have a conserved tripeptide starting with a proline (P30 in cytochrome c) whose carbonyl group accepts a hydrogen bond from N^d of the histidine heme axial ligand. This aligns with the sequence -PDL- in cytochromes c_1 (with the exception of *Bacillus*, which has PSL, and *Rhodobacter sphaeroides*, which apparently has ADL here). The conserved leucine projects into the heme environment and contributes to its hydrophobicity.

A PXL tripeptide is also present in cytochrome c_8 , but not in cytochrome c_6 . The structure for cytochrome c_6 is available and this region is quite different from that of cytochrome c_1 , c , and c_2 , with the carbonyl oxygen of R22 hydrogen bonding the heme ligand histidine.

A basic residue or two at 8 to 9 residues after the conserved P may also be a general feature involved in hydrogen bonding with a heme propionate directly or through a water molecule. In cytochrome c_1 , R120 ion pairs with one heme propionate and, in cytochrome c , R38 does the same.

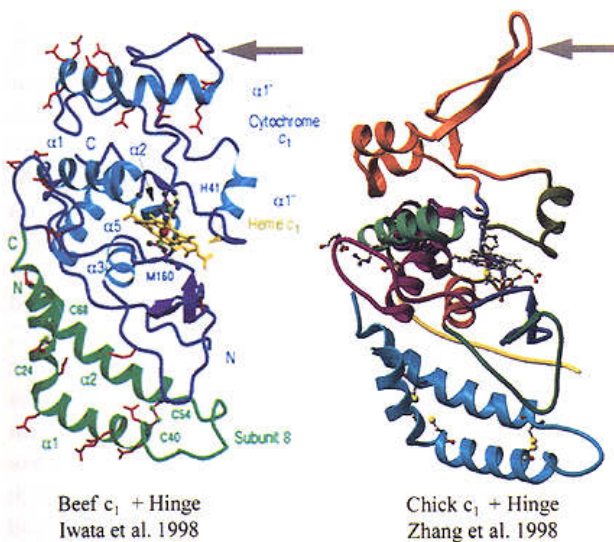


Fig. 9. Comparison of cytochrome c_1 and hinge protein from the orthorhombic crystals of chicken bc_1 (1bcc) with that from the P6₃,22 bovine enzyme (1be3). The bovine structure is on the left; the chicken structure is on the right. A significant difference (described in the text) is indicated by the gray arrow. Because this area has poor order in both structures, the difference could be due to mistracing the polypeptide chain as well as to crystal packing or species differences.

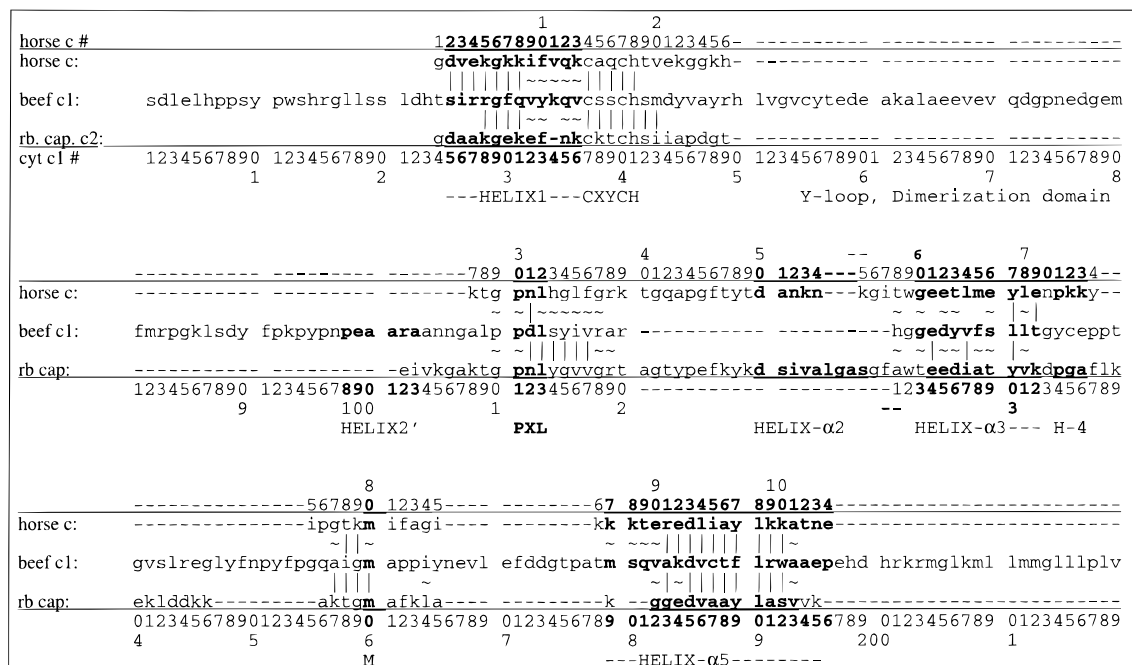


Fig. 10. Structure-based sequence alignment of cytochromes c_1 , c , and c_2 . The sequences are vertebrate cytochrome c_1 (1BCC, middle sequence), mitochondrial cytochrome c (equine 1HRC, top sequence), and bacterial cytochrome c_2 [*Rhodobacter capsulatus* (rb. cap.) 1C2R, bottom sequence]. The symbols between the lines indicate closeness of superposition of C- α atoms of the aligned residues: (|) 1 Å or less, (~) between 1 and 2 Å. The sequence numbering of the beef cytochrome c is indicated above, while that of bovine cytochrome c_1 below, the alignment.

MAJOR DIFFERENCES BETWEEN CYTOCHROME c_1 AND CYTOCHROME c OR c_2

Class I cytochromes have a variable N-terminal extension before helix $\alpha 1$. In mitochondrial cytochrome c , this is 1–5 residues. In cytochrome c_1 , this is much longer. Residues 1–13 run parallel to the terminal helix of the hinge protein (subunit 8). Interestingly, the *Paracoccus* cytochrome has a long acidic insertion in this region, which perhaps performs the function of the mitochondrial hinge protein in this species (Ludwig *et al.*, 1983). Between residue 13 and the start of helix 1 there is a loop reaching into the membrane region, apparently serving as a second membrane anchor. Residues 17 and 18 at the tip of the loop are hydrophobic or proline in all cytochromes c_1 . In the chicken structure, the backbone of residue 17 makes Van der Waals contact with the ring of F246 of cytochrome b of the same monomer.

Between the heme-binding “fingerprint” -CXXCH- sequence and the heme-bracing proline, cytochrome c_2 has six more residues than cytochrome c and cytochrome c_1 has a branched insertion of 58

residues (50–107) between residues 26 and 27 of mitochondrial cytochrome c . One branch, residues 48–67, is mainly helical and folds back against the globular domain of cytochrome c_1 . These include acidic residues around 70 implicated in binding cytochrome c (Stonehuerner *et al.*, 1985). The second branch of the insert, residues 65–87, makes a loop that interacts with cytochrome c_1 in the other monomer: residues 77–78 at the tip of this loop contact residue N97 in the other monomer. This branch was modeled as a two-stranded beta sheet in the chicken structures 1BCC and 3BCC, but as alpha helix and coil in the bovine structures 1BE3 and 1BGY. The carbonyl oxygen of G78 in the turn between beta strands makes a hydrogen bond with N97 of the other cytochrome c_1 in the dimer. These two residues are highly conserved and could be taken as an indication of this same interaction in bovine and other cytochromes c_1 .

Residues 98–103 form two turns of α -helix, which we label $\alpha 2'$, with no corresponding structure in other class I cytochromes. Interestingly, there is a 9–10 residue deletion in the *Rhodobacter* and *Paracoccus* cytochromes that aligns with this helix, suggesting they have the rest of the bifurcated insertion,

the small cytochromes could be derived from cytochrome c_1 or the loop could have been independently lost in different evolutionary branches. Surprisingly, *Rhodobacter* and *Paracoccus* have an insert here only one residue shorter than that of cytochrome c (but with no sequence homology to that of cytochrome c). If it folds, as in cytochrome c , it would interfere with electron transfer from the Rieske cluster, unless there are major structural differences. This may represent an intermediate state in which the loop has moved out of the way to open up the heme propionate exposure, but has not yet been deleted from the sequence.

Between helix 3 and the methionine heme ligand cytochrome c_1 has more residues than cytochrome c or c_2 . The positions and secondary structures are quite different; cytochrome c_1 having no helix corresponding to helix 4 of cytochrome c . Between the methionine ligand and helix 5 cytochrome c_1 is again longer and the insert includes acidic residues 167 and 170 implicated in cytochrome c binding (Broger *et al.*, 1983).

In cytochrome c , helix $\alpha 5$ continues to the C-terminus. Cytochrome c_2 lacks the residue corresponding to the C-terminus of cytochrome c , and the two residues before that are not in the helix, so that $\alpha 5$ is shorter by one turn on the C-terminal end as well. In cytochrome c_1 , the helix $\alpha 5$ continues to the C-terminus of cytochrome c (residue 195 in c_1) then has a turn and begins helix $\alpha 6'$ (the transmembrane helix) with residue 198. On the matrix side of the membrane, residues 233–238 form one strand of an antiparallel beta sheet together with one strand from subunit 7 and six strands from subunit 1.

ACKNOWLEDGMENTS

Diffraction data, including some unpublished data sets, was collected at Stanford Radiation Laboratory (SSRL), which is funded by the Department of Energy, Office of Basic Energy Sciences. The SSRL Biotechnology Program is supported by the National Institutes of Health, National Center for Research Resources, Biomedical Technology Program and the Department of Energy, Office of Biological and Environmental Research. The authors' research is supported by the Office of Biosciences and Environmental Research,

U.S. Department of Energy and by The National Institutes of Health, award R01DK44842 to EAB.

REFERENCES

- Brandt, U., and von Jagow, G. (1991). *Eur. J. Biochem.* **195**, 163–170.
- Brandt, U., Haase, U., Schagger, H., and von Jagow, G. (1991). *J. Biol. Chem.* **266**, 19958–19964.
- Broger, C., Salardi, S., and Azzi, A. (1983). *Eur. J. Biochem.* **131**, 349–352.
- Brugna, M., Albouy, D., and Nitschke, W. (1998). *J. Bacteriol.* **80**, 3719–3723.
- Gray, K. A., Dutton, P. L., and Daldal, F. (1994). *Biochemistry* **33**, 723–733.
- Iwata, S., Lee, J. W., Okada, K., Lee, J. K., Iwata, M., Rasmussen, B., Link, Th. A., Ramaswamy, S., and Jap, B. K. (1998). *Science* **291**, 64–71.
- Keilin, D., and Hartree, E. F. (1940). *Proc. Royal Soc. Ser. B Biol. Sci.* **129**, 277.
- Kim, C. H. and King, T. E. (1983). *J. Biol. Chem.* **258**, 13543–13551.
- Kim, C. H., and King, T. E. (1981). *Biochem. Biophys. Res. Commun.* **101**, 607–614.
- Kim, C. H., and King, T. E. (1987). *Biochemistry* **26**, 1955–1961.
- Kim, H., Xia, D., Yu, C.-A., Xia, J.-Z., Kachurin, A. M., Zhang, L., Yu, L., and Deisenhofer, J. (1998). *Proc. Natl. Acad. Sci. U.S.A.* **95**, 8026–8033.
- Kim, H., Xia, D., Yu, C.-A., Xia, J.-Z., Kachurin, A. M., Zhang, L., Yu, L., and Deisenhofer, J. (1998). *Proc. Natl. Acad. Sci. U.S.A.* **95**, 8026–8033.
- Konig, B. W., Schilder, L. T. M., Tervoort, M. J., and van Gelder, B. F. (1980). *Biochim. Biophys. Acta* **621**, 283–295.
- Ludwig, B., Suda, K., and Cerletti, N. (1983). *Eur. J. Biochem.* **137**, 597–602.
- Mukai, K., Yoshida, M., Toyosaki, H., Yao, Y., Wakabayashi, S., Matsubara, H. (1989). *Eur. J. Biochem.* **178**, 649–656.
- Rieske, J. S. (1967). *Methods Enzymol.* **10**, 239–245.
- Rieske, J. S., Zaugg, W. S., and Hansen, R. E. (1964). *J. Biol. Chem.* **239**, 3023–3030.
- Rieske, J. S., Baum, H., Stoner, C. D., and Lipton, S. H. (1967). *J. Biol. Chem.* **242**, 4854–66.
- Stonehuerner, J., O'Brien, P., Geren, L., Millett, F., Steidl, J., Yu, L., and Yu, C.-A. (1985). *J. Biol. Chem.* **260**, 5392–5398.
- Tian, H., Yu, L., Mather, M. W., and Yu, C. A. (1998). *J. Biol. Chem.* **273**, 27953–27959.
- Tian, H., White, S., Yu, L., and Yu, C. A. (1999). *J. Biol. Chem.* **274**, 7146–7152.
- Wakabayashi, S., Matsubara, H., Kim, C. H., Kawai, K., and King, T. E. (1980). *Biochem. Biophys. Res. Commun.* **97**, 1548–1554.
- Yakushiji, E., and Okunuki, K. (1940). *Imperial Acad. (Tokyo)* **16**, 299.
- Yu, C. A., Yu, L., and King, T. E. (1972). *J. Biol. Chem.* **247**, 1012–1019.
- Xia, D., Yu, C.-A., Kim, H., Xia, J.-Z., Anatoly, M., Kachurin, A. M., Zhang, L., Yu, L., and Deisenhofer, J. (1997). *Science* **287**, 60–66.
- Zhang, Z., Huang, L.-S., Shulmeister, V. M., Chi, Y.-I., Kim, K. K., Hung, L.-W., Crofts, A. R., Berry, E. A., and Kim, S.-H. (1998). *Nature* **392**, 677–684.